A study of three-dimensional aspects of vortex shedding from a bluff body with a mild geometric disturbance

By N. TOMBAZIS† and P. W. BEARMAN

Department of Aeronautics, Imperial College of Science, Technology and Medicine,
London, SW7 2BY, UK

Experiments have been carried out to study the three-dimensional characteristics of vortex shedding from a half-ellipse shape with a blunt trailing edge. In order to control the occurrence of vortex dislocations, the trailing edges of the models used were constructed with a series of periodic waves across their spans. Flow visualization was carried out in a water tunnel at a Reynolds number of 2500, based on trailing-edge thickness. A number of shedding modes were observed and the sequence of mode transitions recorded. Quantitative data were obtained from wind tunnel measurements performed at a Reynolds number of 40000. Two shedding frequencies were recorded with the higher frequency occurring at spanwise positions coinciding with minima in the chord. At these same positions the base pressure was lowest and the vortex formation length longest. Arguments are put forward to explain these observations. It is shown that the concept of a universal Strouhal number holds, even when the flow is three-dimensional. The spanwise variation in time-average base pressure is predicted using the estimated amount of time the flow spends at the two shedding frequencies.

1. Introduction

Above some critical Reynolds number, vortex shedding from nominally two-dimensional bluff bodies exhibits certain three-dimensional characteristics, irrespective of how carefully the experiment is carried out. A simple way of quantifying the three-dimensionality is to measure the spanwise correlation length of some property related to vortex shedding, such as fluctuating pressure on the body surface, fluctuating velocity in the wake or local fluctuating lift. For many shapes of bluff body the correlation length at moderate and high Reynolds numbers is equal to just a few body diameters. This length cannot be predicted and the mechanisms responsible for limiting spanwise correlation are not fully understood. A number of authors have presented measurements of the spanwise correlation length for flows with regular vortex shedding. For example, recently Szepessy (1994) has investigated the correlation of vortex shedding from a circular cylinder at a high subcritical Reynolds number. While, on average, vortices are shed parallel to the cylinder axis, he shows that instantaneously there are substantial variations in the phase of vortex shedding over relatively short spanwise distances.

Gerrard (1966*a*) was one of the first to study in detail the three-dimensionality of cylinder wakes. He identified three important ways in which vortex shedding may

---

† Present address: Benetton Formula Ltd, Whiteways Technical Centre, Enstone, Oxfordshire, UK.

deviate from a two-dimensional form: oblique shedding in which vortices are shed at a small angle to the cylinder axis, the splitting or dislocation of vortices of similar sign and the looping of vortices across to the other side of the wake. Experiments by Williamson (1989) on a circular cylinder at Reynolds numbers up to about 150 have shown that two-dimensional vortex shedding may only be obtained if the cylinder end conditions are very carefully controlled. To maintain vortex shedding parallel to the cylinder axis Williamson used suitably angled end plates. Eisenlohr & Eckelmann (1989) and Hammache & Gharib (1991) achieved parallel shedding over the same range of Reynolds number with other types of end constraint. At higher Reynolds numbers it is still important to control end conditions but it is no longer possible to preserve the instantaneous flow in a two-dimensional state. A vortex dislocation, or split, has been shown by Eisenlohr & Eckelmann (1989) to occur when there is a spanwise variation in the frequency of vortex shedding and it is a means by which vortices of similar sign can connect with each other at a boundary between cells with different shedding frequencies. Vortex looping is a stronger form of three-dimensionality in which a vortex moves across the wake to join with one or more vortices of opposite sign. It seems to require an abrupt change in body geometry from one spanwise station to another and examples of where it might occur are at a step change in body diameter, at a free end or where a bluff body meets a wall.

The types of three-dimensional vortex motion most likely to be found in the wakes of nominally two-dimensional bluff bodies are oblique shedding and vortex dislocation. Bearman & Tombazis (1993) visualized the flow in the wake of a two-dimensional blunt-trailing-edge model fitted with end plates and mounted in a water tunnel. The Reynolds number of their experiment, based on trailing-edge thickness, was 2500 and they found that departures from two-dimensional vortex shedding appear to occur at random points along the span and at irregular time intervals. Both oblique shedding and vortex dislocations were observed. At this higher Reynolds number there is three-dimensional motion related to spanwise instabilities of the Kármán vortices (Triantafyllou 1990), smaller-scale three-dimensionality due to shear layer instability (Wei & Smith 1986) and three-dimensional motion associated with turbulence generated in the flow past the bluff body. To what extent these motions interact is unknown. A possibility is that the small-scale motions act as the disturbance to trigger three-dimensional instability modes of the Kármán vortices.

It is well known, for example Bearman (1984), that the phase of vortex shedding along the span of a bluff body can be synchronized by oscillating the body or the flow at the shedding frequency. A certain threshold amplitude has to be exceeded before extensive regions of correlated vortex shedding are achieved. In the present paper we are concerned with shedding from fixed bodies and no external two-dimensional disturbances are imposed.

Since the primary instability mode in the wake of a two-dimensional bluff body is itself two-dimensional, as discussed by Monkewitz & Nguyen (1987), it is reasonable to suppose that two-dimensional numerical simulation schemes should be able to successfully predict bluff-body flows. However, Szepessy & Bearman (1992) measured the fluctuating lift on a thin section of a large-aspect-ratio circular cylinder and found that two-dimensional simulation schemes generally overestimate the root-mean-square value of fluctuating lift, in some cases by substantial amounts. This observation has been substantiated by Graham (1993) who gathered together numerical predictions for circular cylinder flow and compared them with experimental results. He found that above a Reynolds number of 150 the mean and fluctuating forces were generally over-predicted, with the largest differences occurring in the fluctuating lift. It should also be

noted that measured time histories of fluctuating lift show a pronounced amplitude modulation whereas simulated time histories mostly display a constant amplitude, once the flow has settled. While some of the differences between measurement and prediction may be due to problems in modelling turbulence it seems likely that the three-dimensional features of vortex shedding should also be modelled. It is interesting to note that recently several researchers have developed three-dimensional simulation programs to predict nominally two-dimensional bluff-body flow. It was this increasing appreciation of the importance of three-dimensional effects that stimulated the present research.

Since key three-dimensional features of the wake of a nominally two-dimensional body appear apparently randomly in time and space, it was decided in this study to try to control their locations by applying a mild geometric disturbance in the form of a wavy trailing edge. A number of other authors have reported results of investigations of bluff-body flows influenced by geometric disturbances that might also be described as mild. Nuzzi, Magness & Rockwell (1992) studied the effects of body oscillation on vortex formation from a non-uniform cylinder of circular cross-section. The cylinder had a smooth neck at mid span with a diameter 20 % less than that of the uniform part. A number of interesting observations were made including the finding that some kind of frequency forcing can be transmitted in the spanwise direction across the region of non-uniform diameter. The flow behind a circular cylinder with a slightly larger diameter ring attached at midspan has been investigated by Williamson (1992). The vortices shed from the ring were at a lower frequency than those from the rest of the cylinder and as a result vortex dislocations appeared regularly in the flow. The frequency of these dislocations was at the difference between the cylinder and ring shedding frequencies. Borg & Szewczyk (1993) have examined vortex shedding from a circular cylinder fitted with a splitter plate with a wavy trailing edge. Again vortex dislocations were observed.

A major difference between the present investigation and those mentioned above is that it is not immediately apparent that applying a spanwise wave to the trailing edge of a constant thickness blunt-trailing-edge model will affect the vortex-shedding frequency selection process. Two interesting possibilities presented themselves: if the vortex formation length is constant along the span, then the vortices themselves will be wavy or, if the vortices are two-dimensional, then the base pressure is likely to vary along the span since the vortex formation length varies. These and other aspects are studied in the present paper. A preliminary discussion of some of the results from this investigation can be found in Bearman & Tombazis (1993) and a presentation of all the results is available in the thesis of Tombazis (1993).

2. Experimental arrangement

Wind-tunnel and water-flume experiments were carried out on a number of bluff-body models, each with a nose in the shape of a half-ellipse and with a blunt trailing edge which was either straight or in the form of a sinusoidal wave. The basic bluff-body shape used was similar to one studied earlier by Bearman (1965). In the wind-tunnel experiments, the mean chord of the models along their spans was 190 mm and the semi-major axis of the nose section was 120 mm and the semi-minor axis was 15 mm. The remainder of each model was parallel-sided giving a base height of 30 mm. Trip wires were placed at 40 mm from the leading edge and all models were fitted with end plates. Eight models were constructed in order to be able to study the effect on the flow of both base wavelength, L, and base peak-to-peak wave height, w. A diagram of a typical
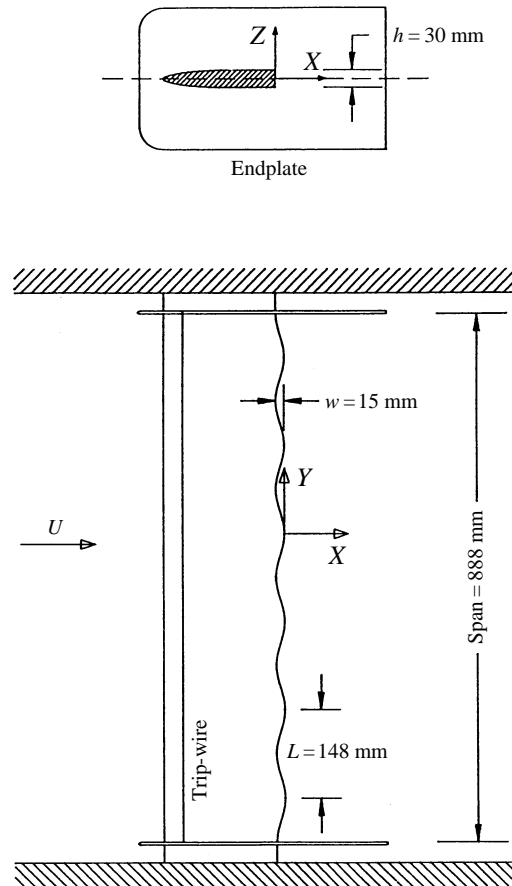
FIGURE 1. Diagram showing the general layout of a typical model and the axis convention used.

model is shown in figure 1. The geometric blockage with a model in the wind tunnel was just over 3% and results were corrected according to the blockage method due to Maskell (1963).

The wind tunnel used is of the closed-return type with a working section 0.91 m × 0.91 m and a turbulence level of less than 0.04%. The Reynolds-number range, using model base height as the reference length, was 20000–60000. The majority of the measurements involved recording mean and fluctuating velocities and pressures using hot-wire anemometry and pressure transducers. Up to seven channels of data were sampled simultaneously and then transferred via a PC to a hard disk for later analysis. Full details of the experimental techniques and the data analysis methods used are given by Tombazis (1993).

Flow visualization was performed at a Reynolds number of 2500 in a water flume with a cross-section 0.6 m × 0.6 m. The models were slightly smaller than those used in the wind tunnel in order to keep the blockage ratios similar. The electrolytic precipitation method described by Honji, Taneda & Tatsuno (1980) was used to visualize the flow. Very thin strips of tin foil were attached to the models and a white precipitate was produced when a suitable potential difference was applied between the strips and the water. Illumination was provided by a light sheet produced from a 5 W continuous argon ion laser. A standard video camera was used to record the flow and, after processing on a workstation, pictures were produced on a laser printer.
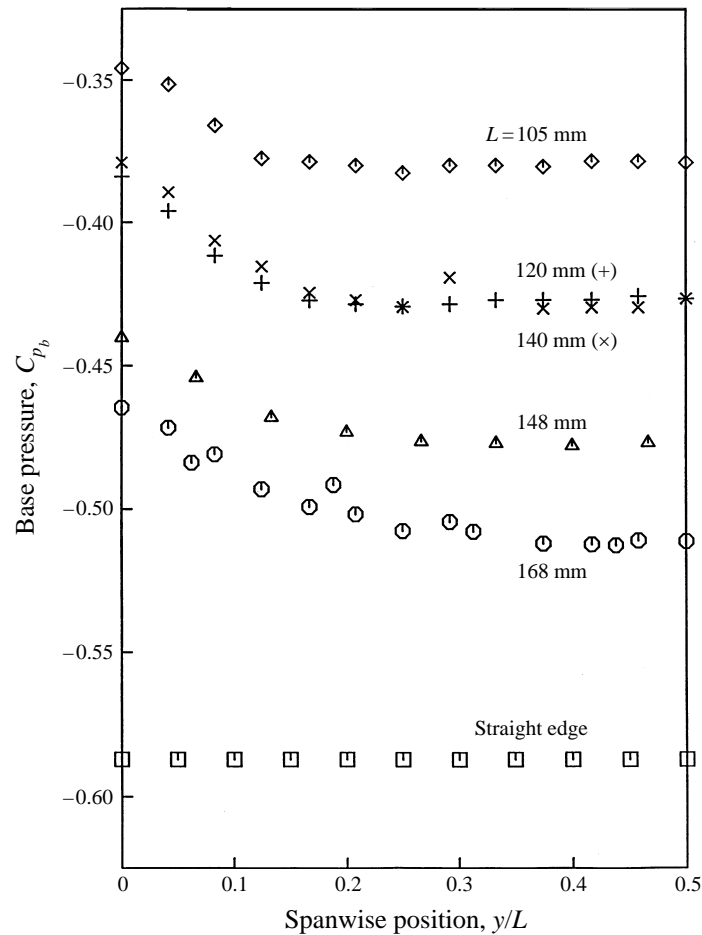
FIGURE 2. Variation of the coefficient of mean base pressure along the centreline of models with different wavelengths but constant wave height. The base pressure coefficient for the straight trailing-edge model is shown for comparison. $h = 30$ mm, $w = 15$ mm.

3. Results

3.1. *Base pressure and Strouhal number measurements*

As an initial comparison between the various models, the spanwise distribution of mean base pressure was measured. For the straight trailing-edge model a constant value of C_{p_b} was found in a spanwise region of $10h$ around the mid-span. The value obtained of -0.585 is in good agreement with previous measurements of Bearman (1965).

Tanner (1972), working with models having a similar cross-sectional shape to the ones studied here, found that by 'breaking' the separation line along the span he could achieve significant drag reduction. In accordance with his results, the wavy models have higher (less negative) values of C_{p_b}. The distributions of base pressure coefficient along a half wavelength of the various wavy models (all with a wave height w of 15 mm) are shown in figure 2. Measurements on all the wavy models showed distributions of base pressure values that repeated themselves over the spanwise waves between the end plates. A notable feature in figure 2 is that the steeper the wave, where steepness $= w/L$, the larger the drag reduction. Compared to the straight-edge model,
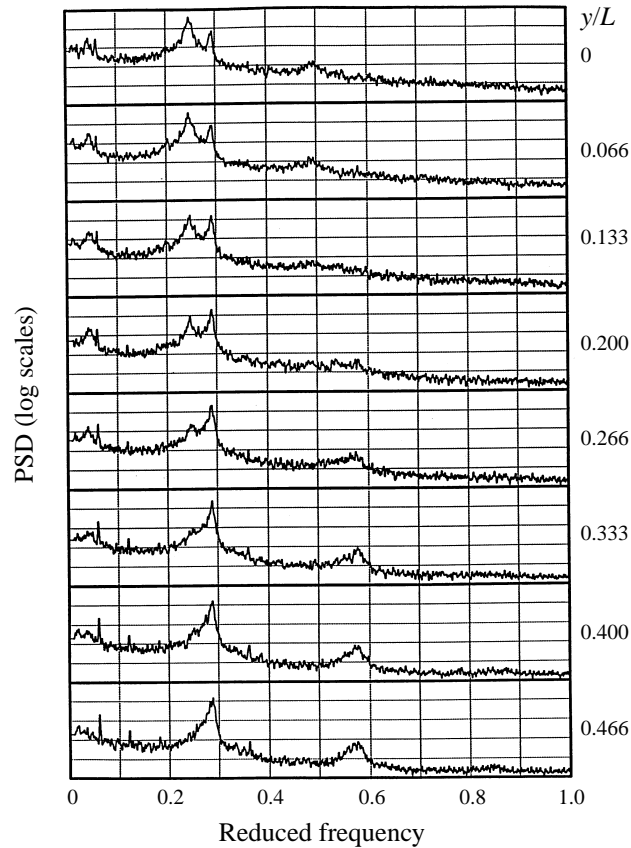
FIGURE 3. Power spectra of velocity measured at $x/h = 0.733$, $z/h = 0.8$ and various values of spanwise position, y/h, for the sinusoidal trailing-edge model with $w/L = 0.1$.

the drag reduction for the models with $w/L = 0.09$, 0.10, 0.11, 0.13 and 0.14 is about 10%, 16%, 24%, 25% and 34% respectively. It is unclear why the difference between the base pressures of the models with wave steepness of 0.11 and 0.13 is so small.

A further important feature of figure 2 is the significant difference between the measured values of C_{p_b} at a peak and a valley. All wavy models show a similar trend, with a peak exhibiting less negative values of C_{p_b} than a valley. For the model with $L = 148$ mm and $w/L = 0.1$, the value at the valley is about -0.48, with C_{p_b} smoothly increasing to a maximum of -0.44 at the peak. It should be noted that from $y/L = 0.2$ to $y/L = 0.5$ (a valley) the base pressure remains quite constant, the main variations being observed for $y/L < 0.2$, i.e. close to the peak.

Power spectra of the velocity records obtained from normal hot-wire probes were calculated in order to determine the characteristic frequencies of the wakes of the various models. The probes were positioned at approximately $0.7h$ downstream of the local trailing-edge position and a distance $0.8h$ above the wake centreline (i.e. outside the shear layer). For the straight-edge model the Strouhal number, obtained using the frequency for the dominant peak in a power spectrum, was 0.24 and this is in agreement with the value obtained by Bearman (1965).

Figure 3 shows velocity spectra for the wavy model with $w/L = 0.1$, measured at different spanwise distances, y, from the peak in a wave. The main characteristic is the presence of two shedding frequencies with one at a Strouhal number of $S = 0.24$ and
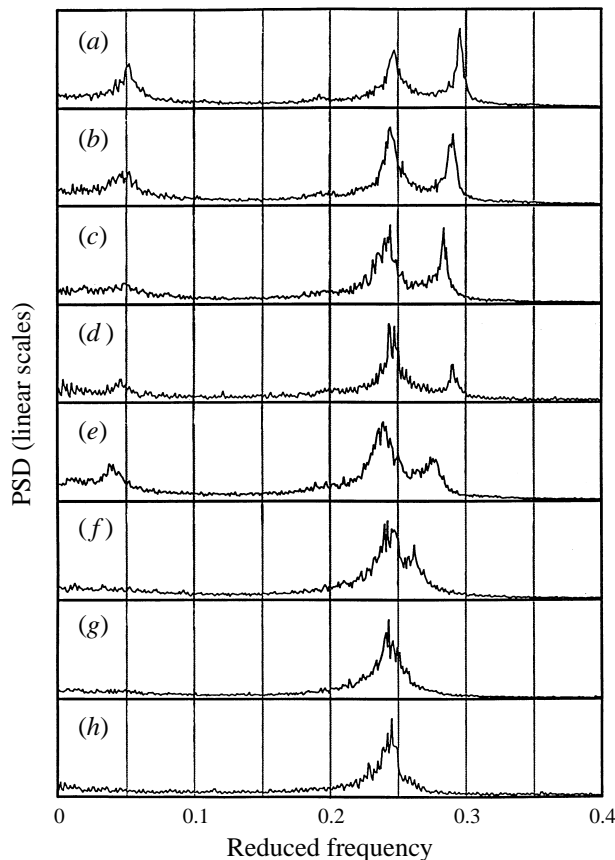
FIGURE 4. Power spectra of velocity measured at a peak for a variety of sinusoidal trailing-edge models: (*a*) $w/L = 0.14$; (*b*) $w/L = 0.13$; (*c*) $w/L = 0.11$; (*d*) $w/L = 0.1$; (*e*) $w/L = 0.09$; (*f*) $w/L = 0.05$; (*g*) $w/L = 0.02$; (*h*) straight trailing edge.

the other at $S = 0.29$. At a peak in the base, the lower of the two frequencies is the stronger, but as we move towards a valley it weakens (becoming almost undetectable at $y/L = 0.333$) and the high-frequency component becomes increasingly strong. The presence of the two frequencies suggests that, at least at some times, we have two cells within this spanwise region, corresponding to a half-wavelength of the trailing edge, shedding at different frequencies. Further, it follows that it is highly likely that there is some form of vortex splitting occurring at the boundary between the cells. The velocity spectra for all wavy models follow a similar pattern. Figure 4 shows spectra measured at the peaks of the various wavy models together with the spectrum for the straight trailing-edge model. As the wave steepness, w/L, increases so the higher of the two shedding frequencies become more and more distinct.

The results presented above were all for $Re = 40\,000$, based on model base height h. Similar measurements were also performed for $Re = 20\,000$ and for $Re = 60\,000$. There was no detectable difference between the results at the various Reynolds numbers. Confirmation that a flow of broadly similar features exists at a Reynolds number an order of magnitude lower was achieved by running the wind tunnel at a very low speed. Although at a Reynolds number of 4000 the hot-wire signal contained a significantly higher proportion of noise, it was still possible to detect the two shedding frequencies. For the remainder of the wind-tunnel investigation it was decided to concentrate
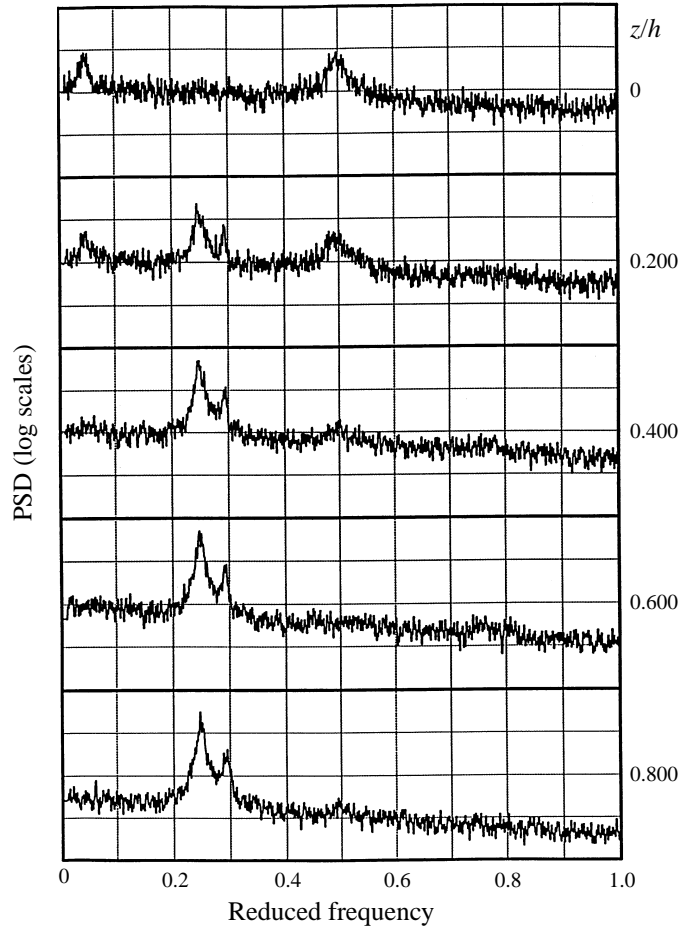
N. Tombazis and P. W. Bearman

FIGURE 5. Power spectra of velocity for the sinusoidal trailing-edge model, $w/L = 0.1$, measured at $x/h = 1.733$, $y/L = 0$ and various positions through the wake.

measurements on one wavy-base model with $w/L = 0.1$ ($L = 148$ mm, $w = 15$ mm) and one Reynolds number ($Re = 40\,000$).

The existence of a dual frequency characteristic has been demonstrated by measuring power spectra of fluctuating velocity but we have to establish what this means from a physical point of view. We cannot be sure that both of the main peaks in a power spectrum of velocity necessarily reflect the frequency of vortex shedding (at some time instants, at least) at that spanwise position. Does the dual frequency indicate a simultaneous presence of two frequencies, e.g. a signal like $C_1 \sin (2\pi f_1 t) + C_2 \sin (2\pi f_2 t)$, or does it represent an interval of $C_1 \sin (2\pi f_1 t)$, followed by an interval at $C_2 \sin (2\pi f_2 t)$? We will return to this point later in the paper.

The spectra plotted in figure 3 were obtained using a hot-wire probe positioned outside the wake but spectra with broadly similar characteristics were observed if the probe was moved into the wake. Although the background spectral levels were higher owing to the presence of turbulence, the peaks related to vortex shedding were still clear. A typical set of spectra from a hot wire placed at various positions through the wake and at $x/h = 1.733$ and $y/L = 0$ is shown in figure 5. An important conclusion arising from the power spectral density measurements is that the dual frequency
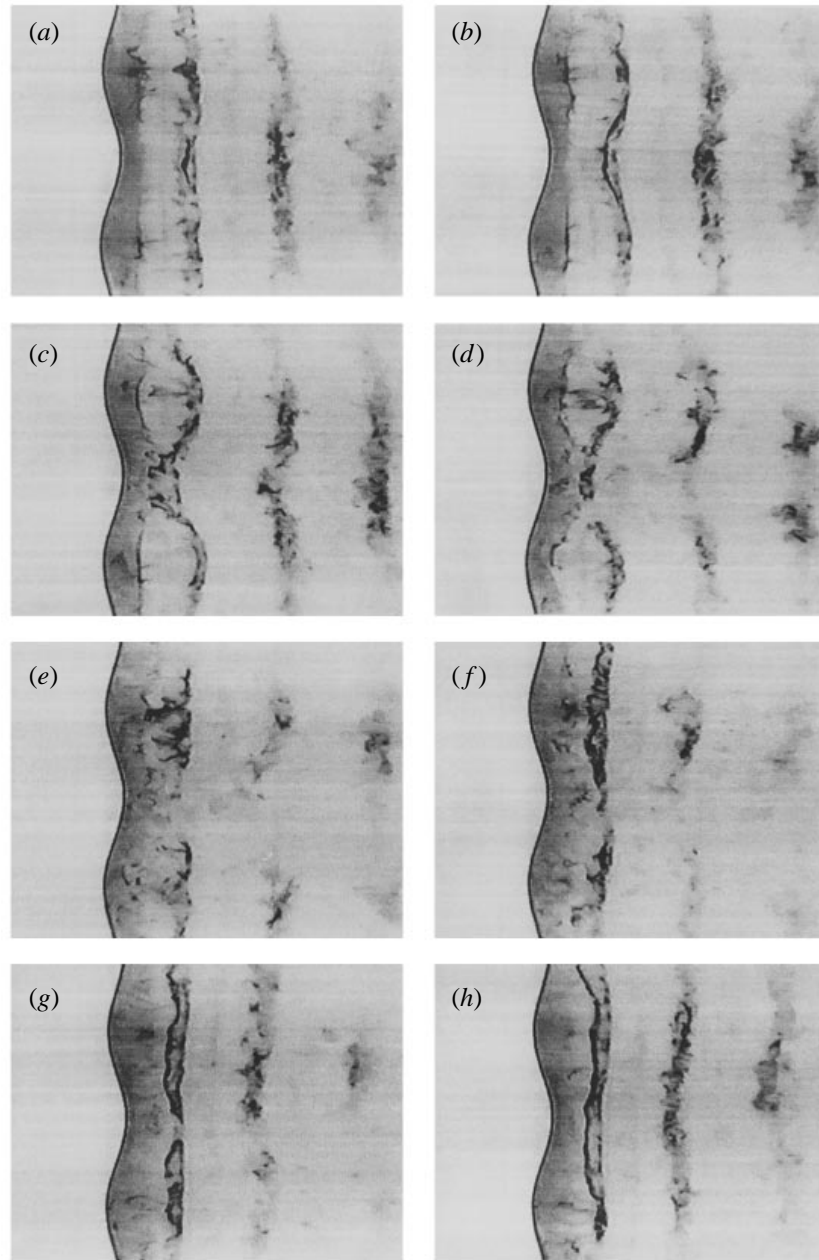
FIGURE 6. Visualization of the wake of the sinusoidal trailing-edge model, $w/L = 0.1$, in the symmetric vortex shedding mode for successive shedding cycles.

characteristic, and the relative energies of the two peaks, are primarily a function of spanwise location rather than the position z/h through the wake.

Returning to figure 4, as wave steepness is increased a third peak appears in the spectra at a reduced frequency of 0.05; i.e. at the difference between the two Strouhal numbers. The presence of this component at the difference frequency, $(f_2 - f_1)$, is most probably due to the simultaneous existence of the f_1 and the f_2 components. However,

the mere presence of these two frequencies is not in itself sufficient to cause the $(f_2 - f_1)$ component. It seems that this apparent 'beat' frequency is the result of a nonlinear interaction of the two shedding frequencies between neighbouring cells.

3.2. *Flow visualization*

Flow visualization performed in the water flume confirmed the cellular nature of the wake of the sinusoidal trailing-edge model. The pictures to be presented in this section give a clear indication that vortex splitting occurs.

Figure 6 shows a sequence which indicates the low-frequency periodicity of vortex splitting. The images were extracted from a video tape, with the shots being roughly one shedding cycle apart. From (*a*) there is little to indicate the complicated three-dimensional nature of the flow. One shedding cycle later, at (*b*), the cell at the peak has delayed its vortex shedding by a small amount. The vortices from the two neighbouring valleys bow backwards to accommodate this delay. At (*c*), another cycle later, a further delay at the peak seems to have brought the two cells out of phase. The vortices from the valleys have bent further back. It appears that when this bowing angle becomes too large then vortex splitting occurs and the vortex from the peak links up with two vortices from each adjacent valley. Eisenlohr & Eckelmann (1989) also identified the large oblique bowing angle as one of the characteristics of vortex splitting. Image (*d*) follows a similar pattern with vortex splitting once again being very pronounced, while from (*e*) to (*h*) the phase difference between the two cells reduces and the vortex filaments then become straight again.

An interesting feature of this flow is the persistent way each cell stays at its selected frequency, acting like an oscillator operating at its own characteristic frequency. Even in figures 6(*a*) and 6(*b*), where the vortices appear to be fairly straight and undisturbed, the cell at the peak is shedding vortices at a slower rate than that at the adjacent valleys. So that even though the flow may at certain instants seem two-dimensional, the underlying physical mechanisms are always three-dimensional.

In the sequence of pictures in figure 6 the flow is symmetric with respect to the peak. Flow visualization revealed a total of four modes, here termed *symmetric*, *antisymmetric* (*two types*) *and oblique*. The oblique mode can be seen in figure 7(*a–d*). From these pictures one can see that there is no preferred positive or negative oblique shedding angle, i.e. the oblique mode is not due to an imperfection in the alignment of the model. During the oblique mode we could reasonably expect a uniform shedding frequency across a peak and an adjacent valley, which may explain the presence of the higher shedding frequency (f_2) in the spectra taken in the wind tunnel at a peak.

In the antisymmetric mode, shown in figure 7(*e–h*), the vortex shedding in the valleys either side of the peak are in antiphase. It is unclear in this mode exactly what is happening in the region of the peak. One possibility is that there are two cells, each associated with a valley and shedding at f_2, that extend up to the peak and link up in that region. Another possibility is that there are three cells with shedding frequencies f_2 at one valley, f_1 at the peak and f_2 again at the other valley. The dislocations would then follow a pattern similar to that for the symmetric mode described earlier. We shall see later that for transition to occur between the symmetric and the oblique modes, both kinds (two-cell and three-cell) of antisymmetric mode must exist.

The flow alternates at seemingly irregular intervals from one mode to another. The transition between the modes does not, as a rule, occur instantaneously, but is gradual. Thus, in order to understand the flow we have to identify possible intermediate states that may accompany the transition from one mode to another. It is unlikely, for example, that the flow will change directly from a symmetric to an oblique mode
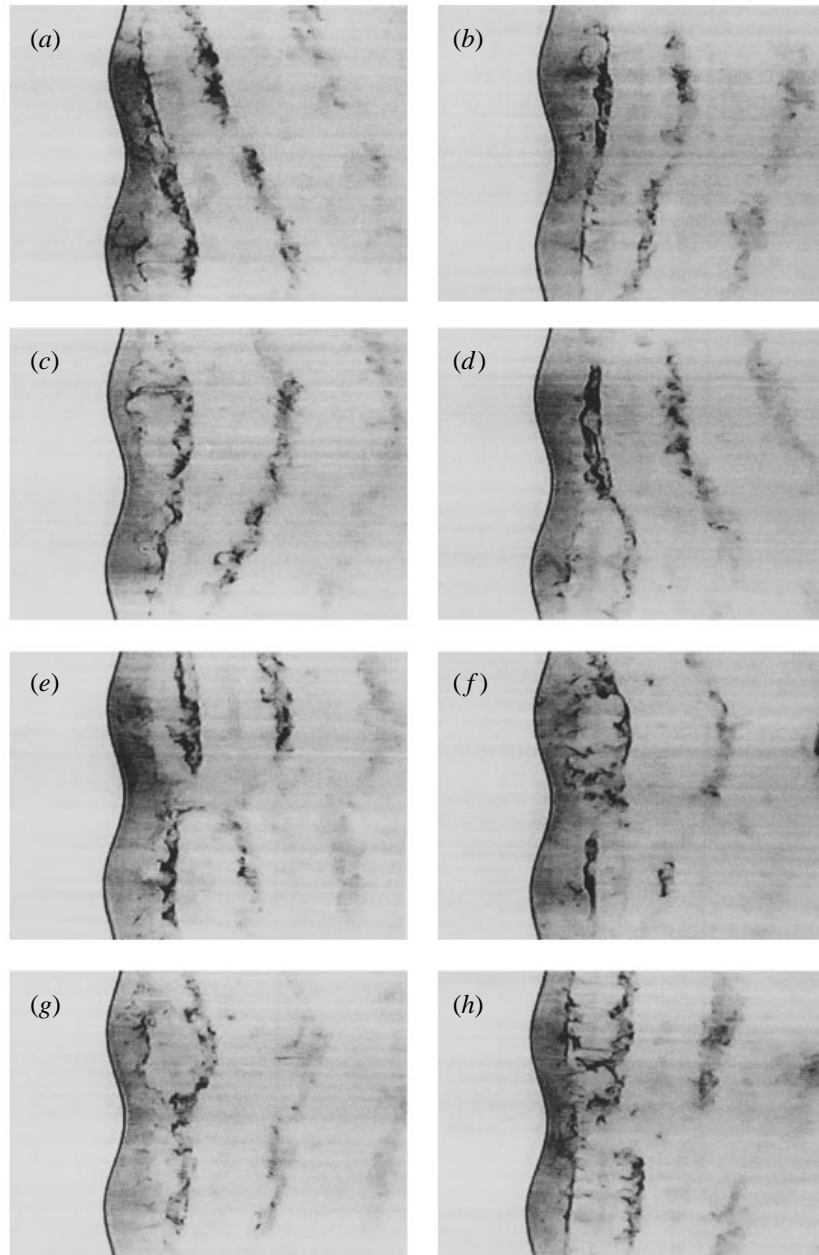
FIGURE 7. Visualization of the wake of the sinusoidal trailing-edge model, $w/L = 0.1$: (*a*) to (*d*) show the oblique vortex shedding mode and (*e*) to (*h*) the antisymmetric vortex shedding mode.

because so many features of the wake would have to change instantaneously. Figure 8 provides paths, derived from detailed study of the flow visualization, for the transitions between modes. The modes are ordered in such a way that each one is above or below the other modes which it most closely resembles. It is suggested that when a mode changes it can only 'jump' between two consecutive boxes of figure 8, either upwards or downwards.

A transition between the symmetric and the three-cell antisymmetric mode would
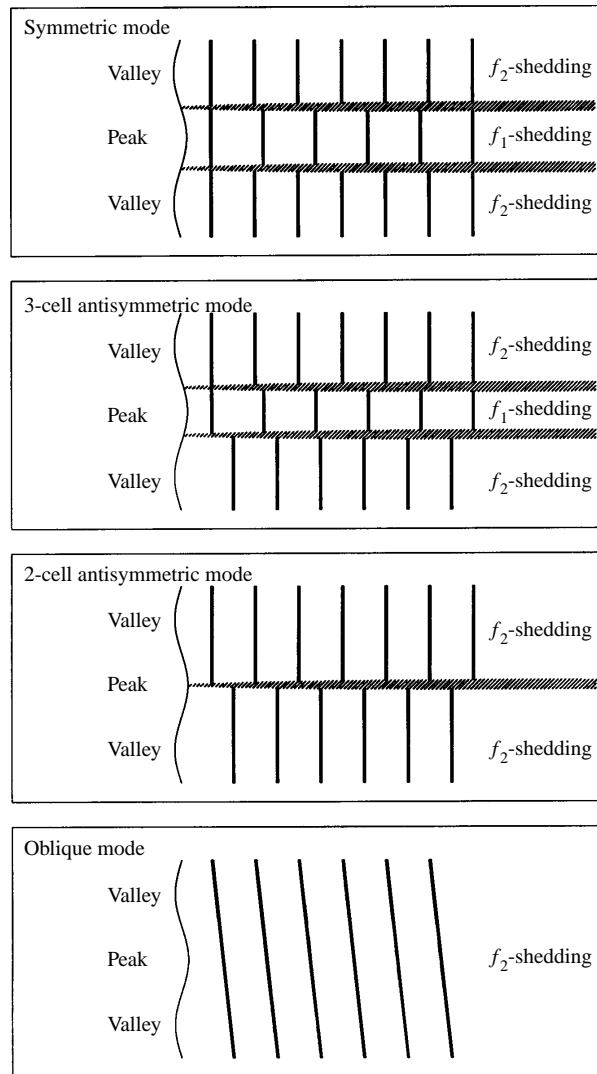
FIGURE 8. Schematic representation of the various shedding modes; shaded areas represent positions where dislocations occur.

involve vortex shedding in the two f_2 cells on either side of the f_1 cell becoming out of phase. The features seen in these two modes are similar to the two-sided dislocations observed by Williamson (1992). He suggests that the velocities induced from one cell with frequency f_2 to the other serve as a means of synchronization between these two cells. One could perhaps apply a similar consideration in the present case, but there is insufficient evidence to support this. What is more likely is that the phase difference between cells is fairly random and the distinction between symmetric and antisymmetric modes is just a broad classification of the flow type. The distinction between the two-cell and the three-cell antisymmetric modes may simply depend on the size of the central (f_1) cell. If at times the central cell shrinks to nothing then we have the two-cell mode and then when it reappears we have the three-cell mode.

Finally, insight into the transition between the two-cell antisymmetric mode and the oblique mode is provided by figure 7(*d*). It is unclear which mode the flow in this image

really belongs to as one could imagine either of the two modes evolving from it. If we have a dislocation separating two cells with the same shedding frequency but different phase, it is conceivable that in the vicinity of the dislocation the vortices straighten out, thus causing oblique vortex filaments.

It was mentioned earlier that the flow would switch between modes at seemingly random intervals. Although a number of mode-transition procedures were proposed above, the actual mechanism of transition is unclear. Obviously a number of questions regarding mode-transition arise. We do not know if the four proposed modes are genuinely 'self-contained' modes. They could each conceal a low-level instability that gradually forces a change of mode. On the other hand, each of the observed modes could be a stable mode, in the sense that, in the absence of external de-stabilizing factors, it could continue *ad infinitum*. In that case the transitions could be triggered by some irregularities in the flow. At the moment one thing is clear: all modes would occur, irrespective of initial conditions and after sufficient time had been allowed for the flow to settle.

Another question concerns the Reynolds number. It would seem possible that the instability causing mode transition could be Reynolds-number dependent. We should therefore treat the existence of the four modes with caution, and not automatically assume their presence at the higher Reynolds number of the wind-tunnel experiments.

3.3. *The relation of the shedding frequency to the mode*

The previous section included some speculation as to how the shedding frequency is related to the mode of vortex shedding. An attempt was made to determine this relation in the wind tunnel. Single hot wires were placed just outside the wake at consecutive valleys. The phase difference between the two signals would determine whether the flow was in a symmetric or an antisymmetric/oblique mode. To distinguish between the two kinds of antisymmetric modes and also to determine whether we had an oblique mode would have been very interesting, but would have required many more hot-wire probes in the flow.

The following criteria were used, regarding the phase difference between the two hot-wire signals:

$(-\frac{1}{12}\pi) < \theta < (\frac{1}{12}\pi)$:   symmetric mode;

$(\pi - \frac{1}{12}\pi) < \theta < (\pi + \frac{1}{12}\pi)$:   antisymmetric/oblique modes (collectively referred

to as 'antisymmetric mode').

The flow would spend about 40 % of the time in each of the modes defined above and 20 % in some intermediate condition. To obtain the power spectrum of the velocity signal $v(t)$ when the flow was in the symmetric mode, a window function $W(t)$ was defined as follows:

symmetric mode not present: $W(t) = 0$;

symmetric mode present: $W(t) = k$ (a normalizing factor).

The transition from 0 to k and from k to 0 was taken as a smooth cosine function. The value of k was determined by ensuring that the root-mean-square value of $W(t)$ was unity. Hence the power spectrum of the signal while the flow was in the symmetric mode was taken as the power spectrum of $v(t) W(t)$. Owing to the low-frequency fluctuations of $W(t)$, the low-frequency components of the resulting power spectrum are not characteristic of the flow fluctuations while shedding is in the symmetric mode.
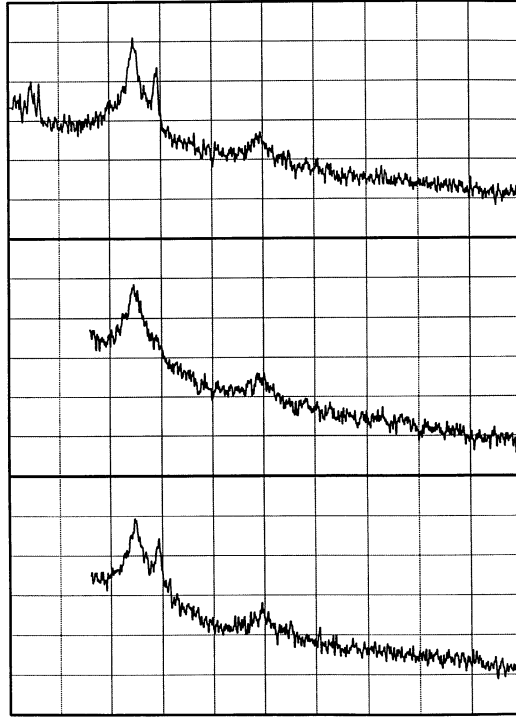
FIGURE 9. Power spectra of velocity for the sinusoidal trailing-edge model, $w/L = 0.1$, measured at $x/h = 0.733$, $y/L = 0$ and $z/h = 0.8$. The upper spectrum is for the whole signal, middle spectrum the symmetric mode part and the lower spectrum the antisymmetric mode part.

The higher frequencies, however, retained their true values. An equivalent procedure was used to obtain spectra for the antisymmetric mode.

Not surprisingly, the most interesting features were observed in the region of a peak of the wavy base. Figure 9 shows spectra obtained at $y/L = 0$ (i.e. at a peak). The most significant finding is that for the symmetric mode the high-frequency component, f_2, is not present. This appears to be strong supporting evidence that the dual frequency characteristic in the spectra is the result of the flow switching between frequencies f_1 and f_2. For the particular mode in question (the symmetric mode) it effectively excludes the possibility of parallel shedding. If the shedding in two valleys is in phase, there must then definitely be a lower-frequency cell in between.

The spectrum for the antisymmetric mode is less informative. When compared to the spectrum of the whole signal, the only notable feature appears to be the small increase of the f_2 component relative to the f_1 peak. It is not surprising that the spectrum for the antisymmetric mode still has both peaks since we had already observed that the mode detection technique could not distinguish between the two antisymmetric modes and the oblique mode. It is, of course, possible that the peak in the spectrum at f_2 is primarily due to induced velocities from vortices in adjacent higher-frequency cells. A similar mode-splitting analysis technique was applied to base pressure fluctuations measured at a peak. In the antisymmetric mode the $2f_2$ component was either absent or too weak to detect while components at $2f_1$ and $f_1 + f_2$ were clearly visible. This adds support to the suggestion that the f_2 component in the velocity signal measured in the antisymmetric mode is much more the result of an induced velocity from an adjacent cell and less an indication of vortex shedding at this frequency at a peak.

We conclude that the occurrence of the two-cell antisymmetric mode and the oblique mode must be relatively rare at the high Reynolds number of the wind-tunnel experiments. In the low-Reynolds-number water-flume experiments they appeared quite often. The presence of the oblique mode at low Reynolds numbers has been observed behind a circular cylinder by other investigators (e.g. Gerrard 1966*a*). Henceforth, if not otherwise specified, the term 'antisymmetric mode' will mean the three-cell antisymmetric mode observed in the water flume. The f_2 component in the antisymmetric mode spectrum of figure 9 is therefore mainly the result of a velocity induced by vortex shedding at another part of the span. Its presence (and its absence from the symmetric mode spectrum) could indicate that the f_1 cell is larger in spanwise extent in the symmetric mode than it is in the antisymmetric mode.

3.4. *Measurement of the mean formation length and mean wake width*

A vortex grows by being fed with vorticity from a connected shear layer. During formation the position of its centre remains more or less fixed relative to the body. As described by Gerrard (1966*b*), when the vortex becomes strong enough to draw the opposing shear layer across the wake, entrainment of opposite-sign vorticity interrupts the feeding of vorticity to the growing vortex. It is at this instant that we can say that the formation process has finished and the vortex is about to be shed.

There now arises the question as to how to determine the formation position experimentally, for each spanwise position. A hot wire was arranged to traverse the wake covering a dense grid (cell size $= 0.1h \times 0.1h$, local $x_{min} = 0.33h$, local $x_{max} = 1.93h$, $z_{min} = 0$, $z_{max} = 0.8h$) for different values of y (spanwise position). The probe axis was parallel to the y-axis, so that it would record velocities induced by the predominantly y-oriented Kármán vortices. Using these measurements, it is not possible to determine rigorously the formation position and hence some assumptions need to be made.

If, for a given spanwise section, we consider the circulation flux passing through a line in the z-direction, we may say that the point of maximum flux is related to the point along this line where the velocity fluctuations at the vortex-shedding frequency are a maximum. Let us assume that these two points coincide. Thus, for each spanwise section and for each streamwise position we can determine the point along the z-direction where there is the maximum flux of circulation. After formation is complete vortices are convected downstream, but they also move slowly away from the wake centreline. Before the position of vortex formation, the shear layer is drawn inwards by the low pressure in the near wake. We can thus conclude that the formation position is the x-wise point where the separation in the z-direction between the maxima in circulation flux is a minimum. The procedure for determining the formation position (which is closely related to that used by Bearman 1965) is shown schematically in figure 10. In figure 10(a), the maxima of the velocity fluctuation intensity curves at various streamwise positions are joined in order to determine the curve of maximum circulation flux. Once this has been obtained, the position of vortex formation is taken to be at the point where this curve is closest to the wake centreline (figure 10*b*).

Using the technique outlined above, the vortex formation length, l_f, and the wake width at formation, w_f, were determined. It was considered advantageous to determine the velocity fluctuation intensity curves for selected frequency ranges and hence the hot-wire signals were analysed by calculating power spectral densities. With the information in frequency bands we could estimate vortex formation positions for each of the two shedding frequencies.

The formation length was estimated for three frequencies: f_1 ($S = 0.24$), f_2 ($S = 0.29$)

(*a*)

Line joining
maxima of
intensity
curves

Fluctuation
intensity
curves

Model section

U_∞

Projected curve

Projection

(*b*)

Formation
length, l_f

Model section

α

Wake
width, w_f

U_∞

Projected curve

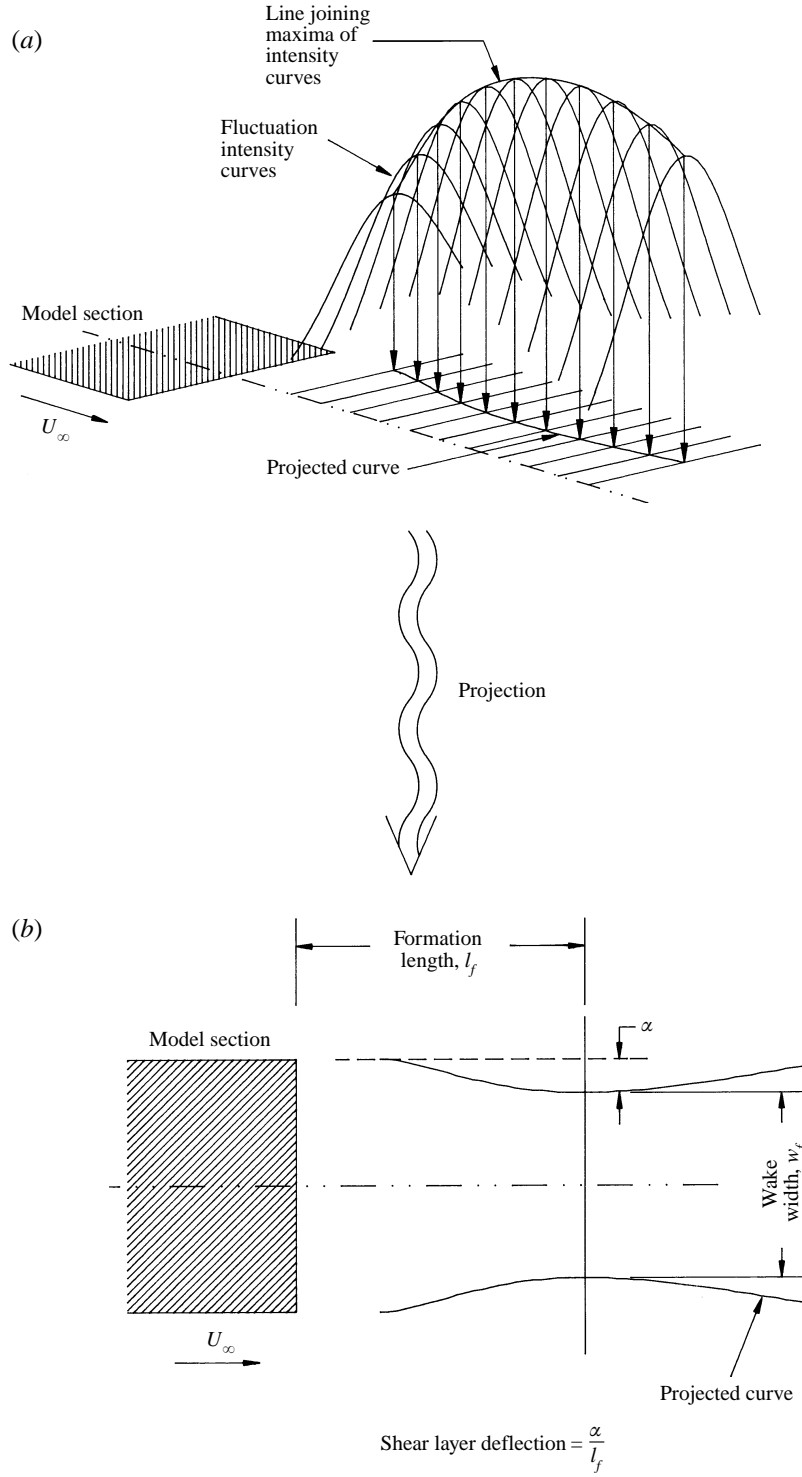$$\text{Shear layer deflection} = \frac{\alpha}{l_f}$$

FIGURE 10. Diagram showing the vortex formation length, the wake width at the vortex
formation position and shear layer deflection.

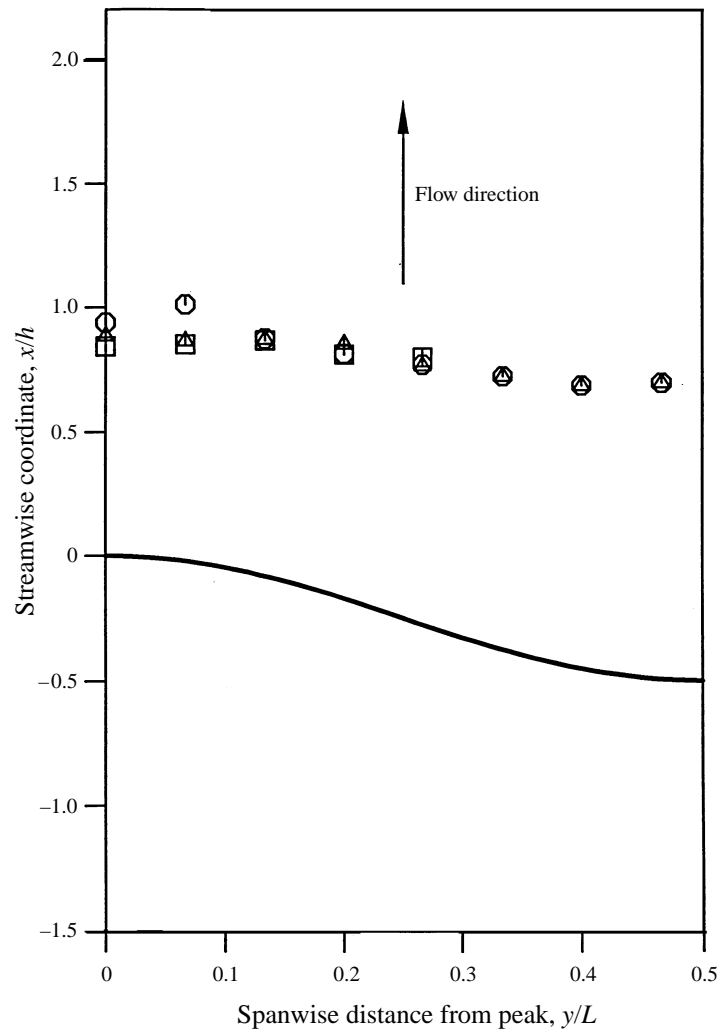FIGURE 11. Vortex formation length versus spanwise distance from a peak in the trailing edge: □, $fh/U = 0.24$; ○, $fh/U = 0.29$; △, average for both frequencies; ————, model trailing edge.

and the combination of these two shedding frequencies. Figure 11 shows vortex-formation position measured from the y-axis together with the profile of the model trailing edge. We can see that the forming vortices have a tendency to straighten out and not follow the exact shape of the trailing edge. The formation distances measured from the model trailing edge are shown in figure 12 where it can be clearly observed that the formation length is longer at a valley than at a peak. Measurements for the two shedding frequencies seem to show similar trends and at most positions it is difficult to distinguish between them. The first two points for the higher shedding frequency ($S = 0.29$), one at a peak and the other just away from a peak, are likely to be quite inaccurate. We have noted earlier that the energy at this frequency is very weak at the peak and much of the signal is due to induced velocity fluctuations from vortices further along the span.
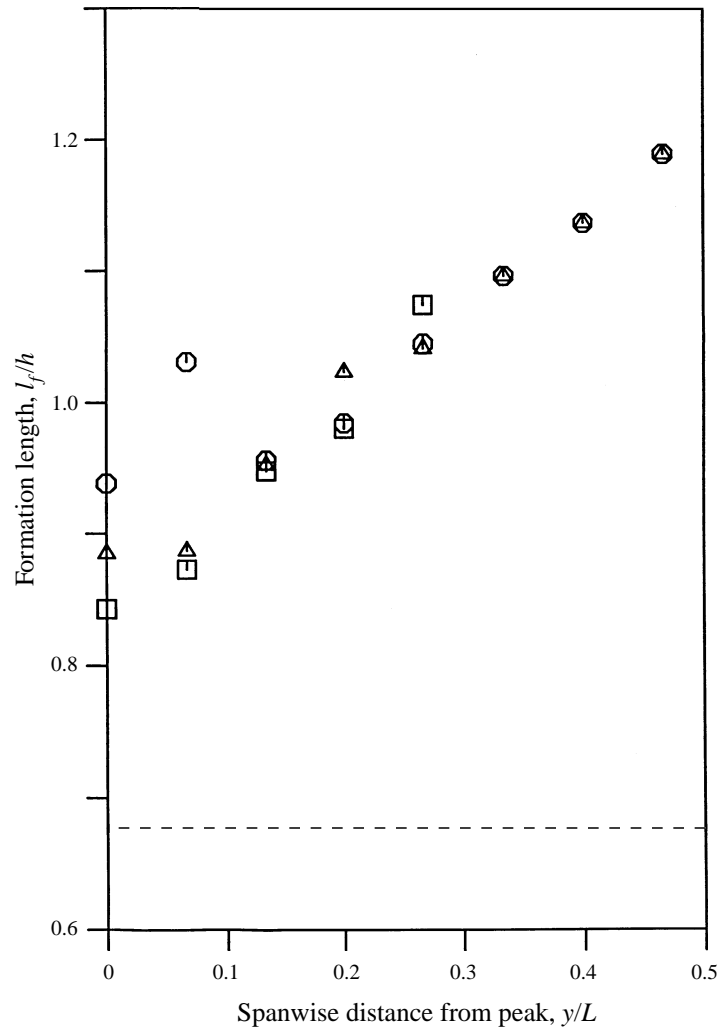
FIGURE 12. Vortex formation length measured from the local trailing-edge position versus spanwise distance from a peak in the trailing edge: □, $fh/U = 0.24$; ○, $fh/U = 0.29$; △, average for both frequencies; ————, vortex formation length for the straight trailing-edge model.

4. Discussion of results

4.1. *On the dynamics of vortex dislocations*

Vortex dislocations are controlled by complex fluid dynamic mechanisms and are a consequence of the fact that vortex lines cannot end abruptly in a fluid. In our discussion of them we will restrict attention to the dynamics of vortices in the near wake; i.e. the region of the flow extending from the base of the body to just beyond the vortex formation position. Dislocations of the vortex structure in the near wake take two distinct forms: splitting and looping. In *vortex splitting* a vortex divides in order to connect to two similar sign vortices on the other side of the dislocation. By its nature, vortex splitting accommodates abrupt spanwise variations in the phase of vortex shedding but we do not expect to find large changes in the circulation flux across such a dislocation. In vortex splitting, vorticity is merely re-distributed into different 'groups'. On the other hand, spanwise variations in circulation flux can be

accommodated by *vortex looping*, whereby a vortex loops across the wake to join with one or more of its opposite-sign counterparts on the other side.

With vortex splitting the redistribution of vorticity happens on the same side of the wake and could even be initiated within the separated shear layer, before the development of fully formed vortices. It appears to be triggered by much milder forms of disturbance than those needed for vortex looping and can even be found behind nominally two-dimensional geometries. Throughout the present study there was no evidence of vortex looping, either in the flow visualization or in the wind-tunnel measurements. Hence, in this paper the term 'vortex dislocation' relates only to vortex splitting.

4.2. *The existence of a characteristic dislocation frequency*

Behind a wavy-based model, neighbouring cells have their own prominent shedding frequency (f_1 and f_2), where $f_1 < f_2$. In the vicinity of a cell boundary a frequency component ($f_2 - f_1$) is also observed and this frequency coincides with the frequency of vortex splitting. We can therefore define the *dislocation frequency f_d* as the frequency difference ($f_2 - f_1$).

Let us now consider the two neighbouring cells, shedding at f_1 (in the region of the peak) and at f_2 (in the region of the valley). In order to accommodate the different numbers of vortices shed in the two cells, vortex splitting must occur at a rate f_d, the characteristic frequency of the dislocation. In the immediate vicinity of the dislocation, we now have to consider what effect vortex splitting will have on the arrangement of the vortices. On the two sides of the dislocation, vortices will sometimes be in phase and sometimes out of phase (the phase difference fluctuating at f_d). When they are in phase their interconnection will be simple, but when they are out of phase vortices will have to bend in some way in order to meet their counterparts on the opposite side of the dislocation. Taking this argument a step further, if we now imagine these two cells gradually getting out of phase, the vortices will have to become more and more bowed. Thus the degree of vortex bowing will change, also at f_d.

The bowing of vortices was observed in the water channel visualization studies. In the sequence shown in figure 7 we can see how the angle of bowing increases from pictures (*a*) to (*d*), as the cell at the peak starts to lag behind its neighbours in its shedding of vortices. When vortex splitting occurs, the cell at the peak finds itself leading suddenly rather than lagging in phase. Thus, from (*e*) to (*h*) the shedding phase difference decreases, with the bowing getting less and less pronounced. This bowing of the vortices in the vicinity of a dislocation will have some effect on the size of the formation region: if at a certain spanwise position the forming vortex has to bend backwards, towards the model, the formation region will become smaller in this cell compared to its neighbour. Similarly, if the vortex bends away from the model, the formation region will grow. As a result, the formation region in the vicinity of the dislocation will fluctuate in size at the characteristic dislocation frequency f_d.

Following the above argument, the base pressure on a wavy model might be expected to fluctuate at the dislocation frequency, in sympathy with the periodic shrinking and expanding of the formation region. Analysis of measurements of unsteady base pressure showed these low-frequency fluctuations to be small but nevertheless a significant feature of the fluctuating part of the signals, particularly at expected positions of dislocations. Now, since the rate of shedding of circulation is related to the base pressure and the base pressure fluctuates at the dislocation frequency then there will be some small fluctuation of vortex strength at the dislocation frequency.
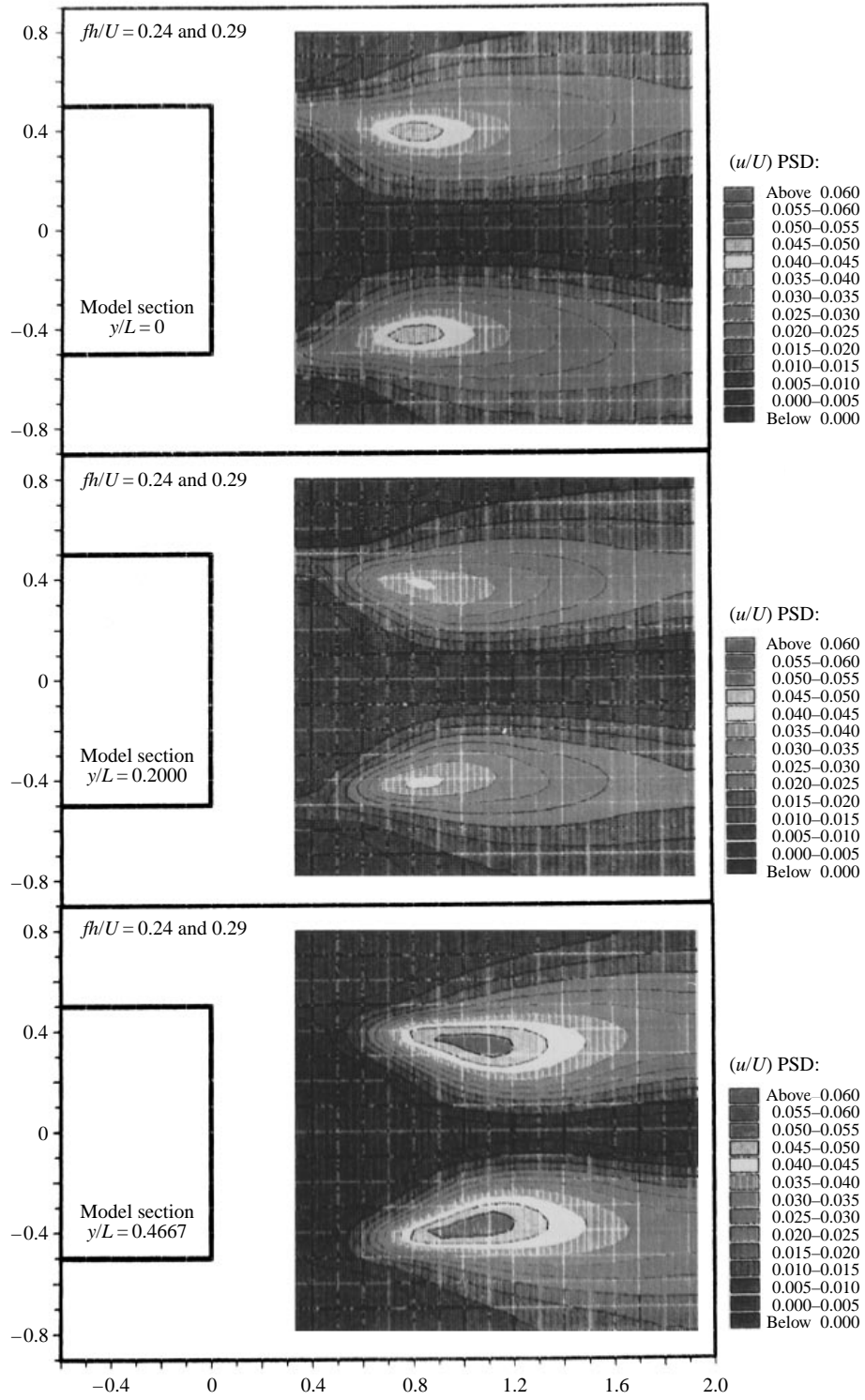
FIGURE 13. Contour plots showing power spectral density levels of velocity for frequencies f_1 and f_2 at three positions across the span of the sinusoidal trailing-edge model, $w/L = 0.1$.

Figure 13 shows contours of the fluctuation intensities measured by the hot wire for the combination of the two shedding frequencies. The results displayed here were used to obtain values for the formation length and the wake width and it is clear that the vortex formation position is further away from the base at the valley than at the peak. In the past, an increase in the formation length has been generally linked to a reduction in base drag. This was observed by many investigators, including Bearman (1965, 1967) who modified the formation length by the use of splitter plates and base bleed, respectively. The argument put forward as to why base drag is reduced is that if the vortex formation length can be increased slightly then the volume of fluid in the recirculation region increases and entrainment of a given amount of fluid out of the base into the forming vortices will be unable to sustain such a low pressure. Further, if the base pressure rises then the rate of shedding of circulation from the body will fall and hence the resulting vortices will be weaker leading to a further reduction in base drag. At the same time, increased formation length means increased entrainment into the shear layers and some new equilibrium state will be reached balancing base pressure, formation length and the entrainment processes. This relation between base pressure and formation length is observed in the present case when we compare the formation length for the straight trailing-edge model (dotted line in figure 12) to the mean formation length for the sinusoidal model. The straight trailing-edge model has a higher base drag which is accompanied by a shorter formation length.

Measurements made on the sinusoidal trailing-edge model, however, seem to contradict the trend discussed above linking the drag to the formation length. Closer study will reveal that this is not a disagreement with the previous theory but its extension into the third dimension. The base pressure C_{p_b} is linked to the velocity at separation by the relation $C_{p_b} = 1 - (u_s/U)^2$, where u_s is the velocity just outside the boundary layer at the separation point. The mean rate of shedding of vorticity from one edge of the model is given by $\mathrm{d}\Gamma/\mathrm{d}t = \frac{1}{2}u_s^2$. Davies (1976) discussed the second-order effect on $\mathrm{d}\Gamma/\mathrm{d}t$ of the fluctuation in u_s and concluded that it was negligible. Some of the shed vorticity is cancelled in the near-wake formation region, while a fraction β survives and contributes to the strength of the formed vortex of that sign. By comparing the rate of flow of circulation in the wake to the rate of shedding of circulation from the body the following expression for β is obtained:

$$\beta = \frac{S\Gamma_v}{\frac{1}{2}Uh(1 - C_{p_b})},\tag{1}$$

where Γ_v is the mean vortex strength just after formation. Note that the nominator here represents the circulation flux carried by, say, positive, Kármán vortices, while the denominator represents the vorticity shed from one side of the trailing edge.

We expect there to be a relation between the vortex formation length l_f and the fraction β. Since entrainment into the shear layers and the mixing of vorticities of opposite signs, leading to vorticity cancellation, increases with l_f, we would expect β to decrease as l_f increases (i.e. $\mathrm{d}\beta/\mathrm{d}l_f < 0$). Considering the continuity of vortex lines, and provided there is no vortex looping, then the circulation flux is not expected to vary along the spanwise direction and so we may write $\mathrm{d}(S\Gamma_v)/\mathrm{d}y = 0$. If we satisfy $\mathrm{d}(S\Gamma_v)/\mathrm{d}y = 0$ then from (1) we obtain $\mathrm{d}\beta/\mathrm{d}C_{p_b} > 0$. Hence, from these two inequalities and taking $C_D \approx -C_{p_b}$, we get $\mathrm{d}C_D/\mathrm{d}l_f > 0$, i.e. local base drag increases with formation length. To explain this qualitatively, where we have a larger formation length there will be more vorticity mixing and cancellation and hence, to satisfy the
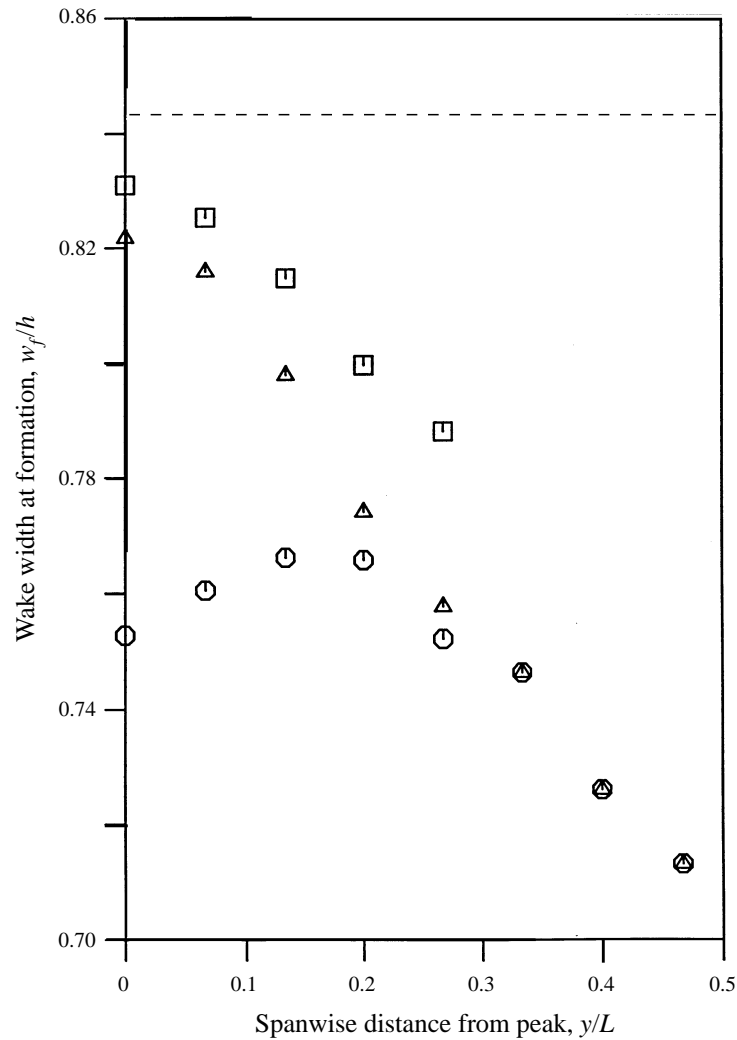
FIGURE 14. Wake width at vortex formation versus spanwise distance from a peak in the trailing edge: $\square$, $fh/U = 0.24$; $\bigcirc$, $fh/U = 0.29$; $\triangle$, average for both frequencies; ————, wake width for the straight trailing-edge model.

condition that the total circulation flux in the formed vortices does not vary along the span, we must have a higher rate of circulation shed at the trailing edge. An increased rate of shedding of circulation implies higher separation velocity and hence higher drag.

4.4. *The wake width and the deflection of the separated shear layer*

There is another issue concerning the relation between formation length and near wake parameters than remains unaddressed. Traditionally, the decrease of base drag with an increase of formation length has been linked to the curvature of the separated shear layer. A shorter formation length usually implies a shear layer curving more rapidly towards the near wake centreline and this increased streamline curvature would have to be balanced by a larger pressure drop across the shear layer.

The curvature of the shear layer does not, however, depend only on the formation length but also on the wake width at formation. For a given formation length, if the
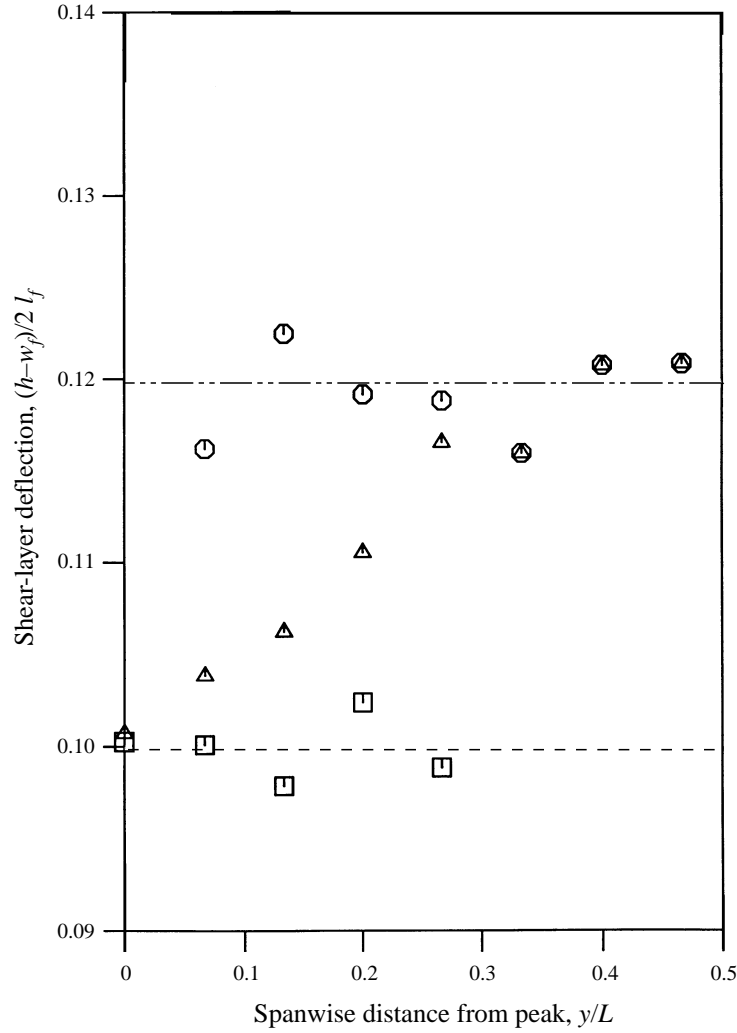
FIGURE 15. Shear-layer deflection versus spanwise distance from a peak in the trailing edge: □, $fh/U = 0.24$; ○, $fh/U = 0.29$; △, average for both frequencies; ————, mean value for $fh/U = 0.24$; ————, mean value for $fh/U = 0.29$.

vortices form closer to the centreline of the wake then the curvature of the shear layer will be larger. Comparing the flow at a peak and a valley, at the valley we have a longer formation length and higher local base drag. Therefore, in order to balance the lower base pressure with a larger shear-layer curvature, we may expect a narrower wake width at vortex formation behind the valleys. This agrees well with the measurements of wake width, averaged over both shedding frequencies, presented in figure 14. The variation between wake widths obtained for the two shedding frequencies will be discussed later.

Shear-layer curvature is a difficult quantity to measure accurately and instead we have estimated the *shear-layer deflection* δ. The definition of this quantity can be seen from figure 10(*b*), where α is taken to be the transverse distance across the wake between the formation position and the point of separation. Now $\alpha \ll l_f$, and hence the shear-layer deflection angle can be taken as $\delta = \alpha/l_f$ (since $\alpha = (h - w_f)/2$, we can define

δ as $(h-w_f)/2l_f$). Shear-layer deflection is thus a relatively easy quantity to measure, but we should remember that it is not quite the same as the shear layer curvature. Therefore, we must be cautious when thinking in terms of a direct relationship between C_{p_b} and δ.

Shear-layer deflection has been plotted against spanwise position in figure 15. Again the trend of the values obtained using data for both shedding frequencies seems to fit in well with the base pressure trend. Figure 15 shows a further interesting result: if we plot values of δ obtained for the two shedding frequencies separately, we can clearly see that the shear-layer deflection at each of these two frequencies is approximately constant. The difference between the two levels is about 20%.

4.5. *The relation of the base pressure to the shedding frequency*

Given the connection between shear-layer deflection and base pressure discussed in the previous section, it is tempting to argue that the shedding frequency is also a function of the base pressure. This implies that base pressure is fairly constant within each cell and that there may be a sharp change in pressure across a dislocation. Should this be the case then the smoothly varying spanwise base pressure distribution shown in figure 2 could result from a rapid pressure change moving back and forth with the dislocation. The mean base pressure at each position would depend directly on how much time the flow there spent at each of the two shedding frequencies.

These times can be obtained by measuring the mean shedding frequency. This was accomplished by counting zero crossings of the velocity signal for large lengths of data. The resulting 'time-averaged' Strouhal number is plotted against spanwise position in figure 16. The dotted lines indicate the two Strouhal numbers ($f_1 = 0.24$ and $f_2 = 0.29$). We can see that the time-averaged Strouhal number lies between those two levels and by interpolation the proportion of time spent at each frequency can be deduced. Note from figure 16 that shedding at the higher frequency is predicted to happen sometimes at a peak, while the lower frequency never occurs at a valley, in agreement with previous observations.

We can now check the simplistic model that for any spanwise position the base pressure alternates between two main levels; the level at any instant depending on which side of a dislocation the measuring point lies. Let us define the two levels to be $C_{p_{b_1}}$ and $C_{p_{b_2}}$. Values for $C_{p_{b_1}}$ and $C_{p_{b_2}}$ were estimated using a least-squares approximation to the known, mean base pressure distribution and found to be $C_{p_{b_1}} \approx -0.432$ and $C_{p_{b_2}} \approx -0.479$. The interpolated, time-averaged base pressure distribution is plotted together with the measured distribution in figure 17. The agreement between the two appears quite good, perhaps justifying our simple model based on a direct relationship between base pressure and shedding frequency. Hence, we can conclude that there is likely to be a strong base pressure gradient across a dislocation. The pressure gradient is thought to be sustained by streamwise vorticity that arises through the bending of vortex filaments in the vicinity of the dislocation.

4.6. *Determination of the time-averaged Strouhal number*

In an attempt to understand why the flow selects two shedding frequencies, first we will consider how the time-averaged Strouhal number could arise. We will use the concept of a 'universal' Strouhal number proposed by Roshko (1954). This concept considers near-wake properties to be the relevant parameters for the selection of frequency, as opposed to global properties. Strouhal number is usually defined by $S = fh/U$, but model height h and the free-stream velocity U are not necessarily the relevant parameters to determine the instability that occurs in the near wake. A more
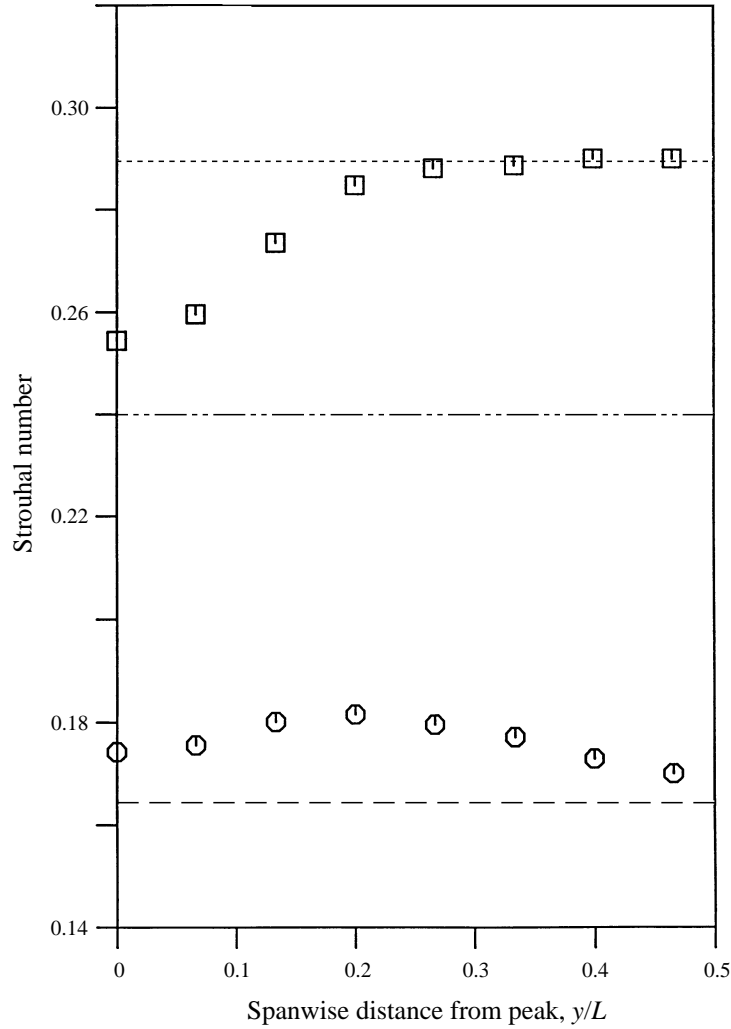
FIGURE 16. Strouhal number versus spanwise distance from a peak in the trailing edge: □, time-averaged Strouhal number; ○, universal Strouhal number, S^*; $-----$, high Strouhal number; $--------$, low Strouhal number; $------$, S^* for the straight trailing-edge model.

appropriate approach that characterizes the vortex-shedding development in the near wake would be to use the local parameters of wake width at formation (w_f) and the velocity outside the wake at the formation position. The latter wake parameter is usually taken to be u_s, the velocity just outside the boundary layer at the separation point. For the present study, we define a 'wake Strouhal number' S^* given by

$$S^* = \frac{Sw_f}{h(1 - C_{p_b})^{1/2}}.$$

The variation of S^* along the span is shown in figure 16. A reasonable collapse of the shedding frequency data is achieved with $S^* \approx 0.17$. The value of S^* obtained for the straight-edge model is quite close to this.
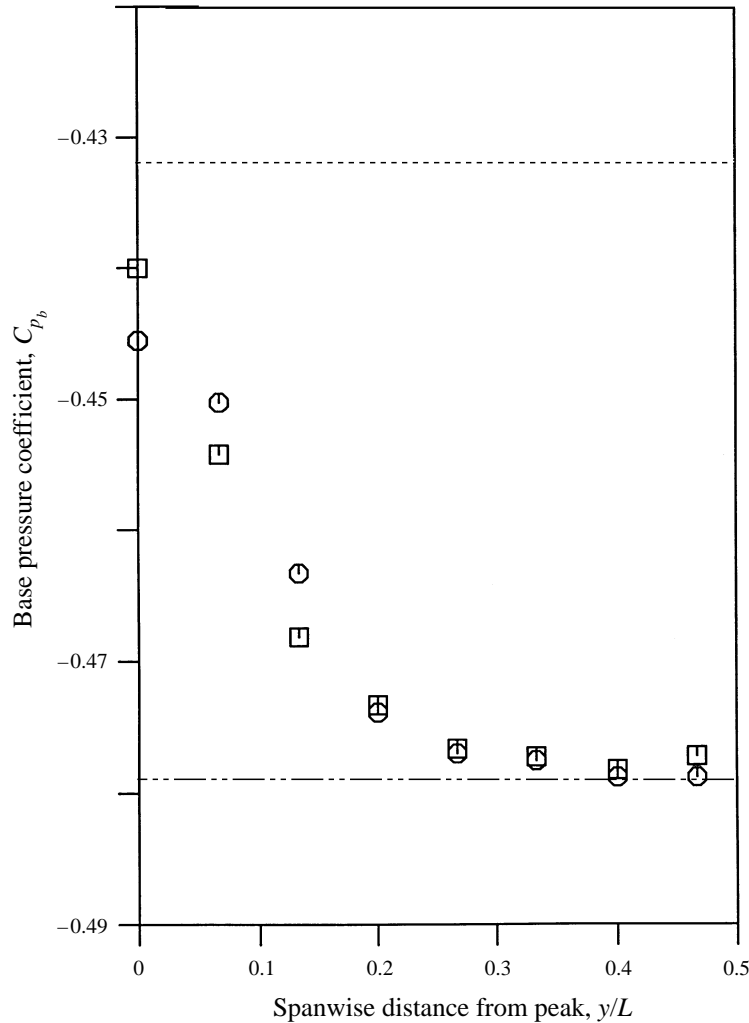
FIGURE 17. Base pressure coefficient versus spanwise distance from a peak: □, measured; ○, interpolated. $------$, estimated value for $S = 0.24$; $--------$, estimated value for $S = 0.29$.

4.7. *Selection of the shedding frequencies*

The similarity arguments applied in the previous section established, given the variations in base pressure and wake width, that there cannot be a single shedding frequency along the span of the sinusoidal model. In this particular case the flow has chosen two shedding frequencies (f_1 and f_2) and alternates between them, with f_1 dominating at a peak (but not completely) and f_2 becoming gradually more prominent and eventually totally dominant as we progress towards a valley.

We can find no obvious explanation for why the flow has chosen two frequencies rather than each spanwise section shedding constantly at the predicted time-averaged frequency. It is conceivable to have such a behaviour with vortices gradually getting out of phase and vortex splitting occurring at various different spanwise positions. This flow perhaps resembling the patterns observed by Gaster (1969) for vortex shedding from slender cones.

A possible explanation might be found by considering some kind of spanwise vortex-shedding 'lock-in'. We can observe from the spanwise distribution of time-averaged

shedding frequency shown in figure 16, that over a considerable portion of a half-wavelength ($0.27 \leqslant y/L \leqslant 0.5$) the time-averaged shedding frequency is constant with $S = 0.29$. It would then seem reasonable to expect that frequency to be chosen as one of the characteristic frequencies of the wake. Consequently, we will have a strong cell shedding at a single frequency. It is possible that under the influence of the induced velocities of that cell other spanwise sections occasionally get 'locked-in' and shed at that frequency. The selection of the second characteristic frequency could then be forced in order to achieve the required value of time-averaged shedding rate for each spanwise position. Once a certain frequency (with $S < 0.29$) has been established over a small portion of the span, it could (under the mechanism of the spanwise lock-in) spread out until the wake is dominated by these two characteristic frequencies.

There is no evidence to support directly these suggestions, apart from the fact that the flow does indeed select two frequencies. Speculating further, it seems plausible that if a balance could not be reached with two frequencies then one or more extra characteristic frequencies might emerge. A considerably more intricate flow pattern would then result with three or more shedding frequencies and multiple combinations of cells. Clarification of these complex issues will have to await further research.

6. Conclusions

Three-dimensional features of bluff-body wakes can be studied in a controlled way by adding a set of wavy trailing edges to a basic blunt-based model. The addition of a wavy trailing edge reduces base drag with the largest reductions occurring at peaks in the waves. The average base pressure across the span rises with increasing wave steepness. Two shedding frequencies were noted, with the higher of the two frequencies being dominant at a valley. Vortex splitting occurs regularly in the region of a peak, but at the two neighbouring valleys vortex shedding can be either in phase or out of phase. A number of modes of vortex shedding are observed and the sequence of transitions between modes has been established.

Measurements of vortex formation length show an unexpected feature with the longest length occurring at a valley where the base pressure is lowest. This is explained by considering the fraction of the shed vorticity that survives vortex formation and arguing that mixing and cancellation must be greater at a valley. Using a suitable wake width and the velocity just outside the boundary layer at separation as characteristic length scales and velocity scales, it is found that the shedding-frequency data at various spanwise stations approaches a universal Strouhal number. By measuring the time-average of the shedding frequency at any station the amount of time the flow spends at each of the two observed shedding frequencies was calculated. A simple model is proposed in which a certain level of base pressure is associated with each shedding frequency so that at a dislocation there will be a jump in base pressure. Dislocations occur at a frequency equal to the difference between the two shedding frequencies and their spanwise positions move, hence the time-average base pressure will show a continuous and smooth distribution across the span. By making use of the times the flow spends at each frequency and knowing the base pressure associated with each frequency, this spanwise distribution of time average base pressure can be predicted well.

REFERENCES

BEARMAN, P. W. 1965 Investigation of the flow behind a two-dimensional model with a blunt trailing edge and fitted with splitter plates. *J. Fluid Mech.* **21**, 241–255.

BEARMAN, P. W. 1967 The effect of base bleed on the flow behind a two-dimensional model with a blunt trailing edge. *Aero. Q.* **18**, 207–224.

BEARMAN, P. W. 1984 Vortex shedding from oscillating bluff bodies. *Ann. Rev. Fluid Mech.* **16**, 195–222.

BEARMAN, P. W. & TOMBAZIS, N. 1993 The effects of three-dimensional imposed disturbances on bluff body near wake flows. *J. Wind Engng & Ind. Aerodyn.* **49**, 339–350.

BORG, J. & SZEWCZYK, A. A. 1993 Unsteady base pressure measurements in the near wake of a cylinder with imposed three-dimensional disturbances. *Bluff Body Wakes, Dynamics and Instabilities*, pp. 39–42. Springer.

DAVIES, M. E. 1976 A comparison of the wake structure of a stationary and oscillating bluff body, using a conditional averaging technique. *J. Fluid Mech.* **75**, 209–231.

EISENLOHR, H. & ECKELMANN, H. 1989 Vortex splitting and its consequences in the vortex street wake of cylinders at low Reynolds numbers. *Phys. Fluid* A**1**, 189–192.

GASTER, M. 1969 Vortex shedding from slender cones at low Reynolds numbers. *J. Fluid Mech.* **38**, 565–576.

GERRARD, J. H. 1966*a* The three-dimensional structure of the wake of a circular cylinder. *J. Fluid Mech.* **25**, 143–164.

GERRARD, J. H. 1966*b* The mechanics of the formation region of vortices behind bluff bodies. *J. Fluid Mech.* **25**, 401–413.

GRAHAM, J. M. R. 1993 Comparing computation of flow past circular cylinders with experimental data. *Bluff Body Wakes, Dynamics and Instabilities*, pp. 317–324. Springer.

HAMMACHE, M. & GHARIB, M. 1991 An experimental study of the parallel and oblique shedding from circular cylinders. *J. Fluid Mech.* **232**, 567–590.

HONJI, H., TANEDA, S. & TATSUNO, M. 1980 Some practical details of the electrolytic precipitation method of flow visualisation. *Rep. Res. Inst. Appl. Mech., Kyushu Univ., Japan*, **28**, 83.

MASKELL, E. C. 1963 A theory of the blockage effects of splitter plates on the wake flow behind a bluff body. *Aero. Res. Counc. R&M* 3400.

MONKEWITZ, P. A. & NGUYEN, L. N. 1987 Absolute instability in the near-wake of two-dimensional bluff bodies. *J. Fluids Struct.* **1**, 165–184.

NUZZI, F., MAGNESS, C. & ROCKWELL, D. 1992 Three-dimensional vortex formation from an oscillating, non-uniform cylinder. *J. Fluid Mech.* **238**, 31–54.

ROSHKO, A. 1954 On the drag and shedding frequency of two-dimensional bluff bodies. *NACA Tech. Note* 3169.

SZEPESSY, S. 1994 On the spanwise correlation of vortex shedding from a circular cylinder at high Reynolds number. *Phys. Fluids* **6**, 2406–2416.

SZEPESSY, S. & BEARMAN, P. W. 1992 Aspect ratio and end plate effects on vortex shedding from a circular cylinder. *J. Fluid Mech.* **234**, 191–218.

TANNER, M. 1972 A method of reducing the base drag of wings with blunt trailing edges. *Aero. Q.* **23**, 15–23.

TOMBAZIS, N. 1993 Effects of three-dimensional disturbances on bluff body near wakes. PhD thesis, University of London.

TRIANTAFYLLOU, G. S. 1990 Three-dimensional flow patterns in two-dimensional wakes. *ASME Symp. on Non-Steady Fluid Dyn.* FED **92**, 395–402.

WEI, T. & SMITH, C. R. 1986 Secondary vortices in the wake of a circular cylinder. *J. Fluid Mech.* **169**, 513–533.

WILLIAMSON, C. H. K. 1989 Oblique and parallel modes of vortex shedding of a circular cylinder. *J. Fluid Mech.* **206**, 579–627.

WILLIAMSON, C. H. K. 1992 The natural and forced formation of spot-like 'vortex dislocations' in the transition of a wake. *J. Fluid Mech.* **243**, 393–441.